Detail categories for the flange-to-web weld detail in corrugated web girders

(article starts on next page)

Detail categories for the flange-to-web weld detail in corrugated web girders

Fatima Hlal [a,b,*], Mohammad Al-Emrani [a]

[a] Department of Architecture and Civil Engineering, Chalmers University of Technology, Gothenburg, Sweden
[b] Bridge Department, WSP, Gothenburg, Sweden

ARTICLE INFO

ABSTRACT

Corrugated web girders have gained popularity in both buildings and bridges due to their efficient use of materials. Previous research work has demonstrated that stainless steel corrugated web offers a promising solution for composite road bridges. However, to utilize these girders Efficiently in bridges, it is crucial to understand their fatigue performance. Notably, EN1993–1-9 does not include a detail category for the flange-to-web weld detail in girders with corrugated webs made of either carbon or stainless steel. To address this gap, numerous tests have been conducted and reported in the literature on carbon steel girders with various corrugation geometries. This paper aims at deriving detail categories for the flange-to-web weld detail in girders with corrugated webs. As a first step, it focuses on carbon steel, compiling, analyzing, and evaluating 86 fatigue test results available in the literature. The results show that the corrugation angle is the most important geometric parameter influencing the fatigue strength of the studied details. Based on this work, the following detail categories are proposed for various corrugation angles: DC125 for angles smaller than $30°$, DC112 for angles between $30°$ and $40°$, DC100 for angles between $40°$ and $45°$, and DC90 for angles between $45°$ and $60°$. Furthermore, the impact of other influencing geometrical parameters, such as bend radius and flange thickness, on fatigue strength is explored. The risk for root cracking in the weld between the flange and corrugated web is also evaluated through effective notch stress analysis.

1. Introduction

Beams with corrugated webs have been used in buildings and bridges, proven to be an economical solution [1–3]. The use of corrugated webs allows for thin web plates without additional transverse stiffeners, which significantly reduces material and fabrication costs and produces bridge girders with improved fatigue life [2,4]. While the use of stainless steels in bridges has shown promising results in terms of life cycle cost (LCC) [5–9], high initial investment costs have hindered its widespread adoption in bridge construction [6]. Recent research indicates that incorporating corrugated webs into stainless steel bridge girders can offer a competitive design solution [10]. This approach helps reduce the material cost gap between stainless steel and carbon steel girders while retaining the life cycle cost benefits of stainless steel [10]. Design solutions incorporating corrugated webs decrease material usage, maintenance, and production costs, potentially offsetting the higher material cost of stainless steel [10,11]. However, to utilize corrugated webs in bridge girders, it is essential to define a detail

category that describes the fatigue strength of such girders.

Regarding fatigue behaviour, beams with corrugated webs introduce stress concentration points, typically found at the corners of the corrugations. These points exhibit specific fatigue strength properties and are influenced by load effects that differ from those in flat web girders [12–14]. Previous experimental tests have shown that fatigue cracking frequently appears at the intersection of inclined and flat folds [15–19], represented as the S-point in Fig. 1.

Numerous fatigue tests have been conducted with reference to the weld between the flange and the web in corrugated web beams. With respect to loading, conducted tests can be categorized as follows: beams loaded in four-point bending, beams under three-point bending, and T-section members loaded axially, see Fig. 3.

Ibrahim et al. [18] [20] tested six hybrid girders (flanges and stiffeners of high-strength low-alloy M270–96 and web of light-gauge cold-formed steel $fy = 324 MPa$) under four-point bending. All beams developed cracks in the constant moment zone due to fatigue, with one girder cracking in the middle of the inclined fold due to a weld start-stop point, while all other beams had cracks initiated from an S-point. Sause

* Correspondence to: Department of Architecture and Civil Engineering, Chalmers University of Technology, Sven Hultins gata 6, 412 96 Gothenburg, Sweden.
E-mail address: fatima.hlal@chalmers.se (F. Hlal).

Nomenclature

|			
LCC	Life cycle cost.	a_2	Length of the inclined fold.
CWT	Corrugated web T-section member.	a_4	Projected length of the flat fold along the horizontal axis.
CWG	Corrugated web girder.	a_3	Corrugation depth.
FWT	Flat web T-section member.	N	Number of cycles to failure.
DC	Detail category.	S	Stress range.
GMAW	Gas metal arc welding.	$\Delta\sigma_{nom}$	Nominal stress range.
α	Corrugation angle.	ENS	Effective notch stress.
t_w	Web plate thickness.	σ_{hs}	Hot spot stress.
h_w	Web plate height.	MPC	Multi-point constraint.
t_f	Flange plate thickness.	ENS_{Toe}	Effective notch stress at weld toe.
b_f	Flange plate width.	ENS_{Root}	Effective notch stress at weld root.
R	Corrugation bend radius.	SCF_{Toe}	Stress concentration factor in the weld toe.
a_w	Fillet weld throat thickness.	r	Effective notch radius.
a_1	Length of the flat fold.	M_{max}	Maximum transverse bending moment.
		V	Shear force.
		IIW	International Institute of Welding.
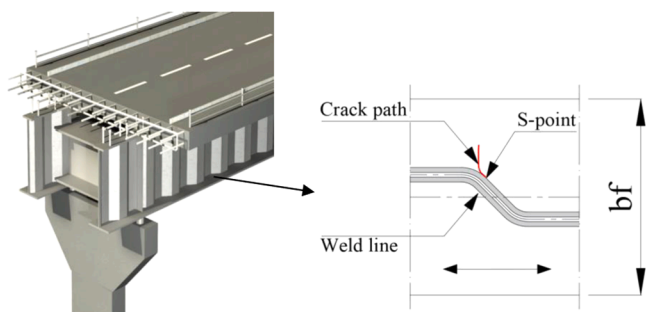
Fig. 1. Typical location of fatigue crack in corrugated web girders.

et al. [21] tested eight large-scale girders with trapezoidal corrugated webs made of HPS 485 W. Six of the girders were welded using semi-automatic gas metal arc welding (GMAW), and two were re-welded using robotic GMAW. The girders that exhibited fatigue failure developed cracks at the S-point in the pure bending area. Kotaki et al. [22] conducted tests on two different corrugated web specimens, each simulating a real bridge with two I-girders. The top flanges were made of SM490YB, while the webs were made of SM400 and the bottom flanges of SM570. Fatigue failure occurred in the constant moment zone. The initial cracks were detected at the S-point or the corresponding point on the other side of the web.

Kövesdi & L. Dunai [15] tested six steel (S355) beams under static and cyclic loading. Two of the beams were tested under 4-point bending and four under 3-point bending. Three girders reached 4 million cycles without fatigue cracks and were considered runouts, while the other three failed under three-point bending with cracks initiating at the S-point in the tension flange. Xu et al. [23] studied a prefabricated specimen with oblique flanges (19.3°) to investigate fatigue performance in box girders with a steel quality of 355GNH for the web and Q345d for the other parts. The girder failed outside the constant moment zone, with cracks initiating at the S-point. However, the first observed cracks were in the constant moment region.

Wang et al. [24] tested four girders made of steel Q345 to analyse the influences of corrugation angle, scallop, and lap joint details. The girder with web having a corrugation angle of 30.6° without scallop failed from a notch in the flange plate edge, while the 45° angle girder developed a fatigue crack at the S-point. Wang et al. [16] also tested 41 corrugated-web T-section members (CWT) with varying corrugation angles (30°, 45°, and 60°). Most specimens failed at S-point, except one that cracked from a notch in the plate edge. Tong et al. [17] investigated fatigue behaviour using trapezoidal corrugated web T-section members

(CWTs) of steel quality Q355. Most fatigue failures occurred at the S-point, though two CWT specimens reached "run-out" after 3 million cycles without crack initiation. In addition to the 18 CWT specimens, one girder tested under four-point bending developed a crack in the pure bending area at the S-point.

Currently, EN1993–1-9 does not provide a detail category for fatigue design of web-to-flange welded connection in beams with corrugated webs. This paper aims at addressing this gap by deriving a detail category for this specific weld detail. Fig. 2 provides an overview of the methodology used, which encompasses the analysis of existing fatigue test results and complementary numerical simulations. Data from previous studies have been gathered, focusing exclusively on fatigue tests for corrugated beams made of carbon steel. Currently, no test data are available for stainless steel. Therefore, as an initial step, this paper aims to establish a detail category specifically for carbon steel corrugated web beams. This data includes different geometrical parameters like corrugation angle, bend radius, and flange thickness. This comprehensive dataset allows for a thorough statistical analysis to establish a detail category and thereafter categorize it based on the corrugation angle. In the numerical study, effective notch stress analysis is then conducted on tests with different angles to verify the applicability of the DC225 proposed by the IIW recommendations [25]. Additionally, the thickness effect is examined using the effective notch stress method to ensure the proposed detail categories are applicable for bridge applications where thicker plates are typically encountered in bridge girders. The risk of root cracking in the studied details is also discussed, and a minimum ratio between weld throat thickness and web plate thickness is suggested to mitigate this risk.

Thus, the significance of this research is that it fills a gap in EN1993–1-9 by proposing a fatigue design category for web-to-flange welded detail in corrugated web beams, specifically based on the corrugation angle. It also discusses the applicability of this category for bridge design, where thicker plates are typical. Moreover, it discusses the risk of root cracking in the studied welded detail, recommending a minimum weld throat-to-web plate thickness ratio to mitigate this risk, offering practical design and fabrication guidelines. These insights contribute significantly to the field.

2. Fatigue assessment methods based on SN curves

Based on SN curves, three fatigue assessment methods can be identified: the effective notch stress approach, the nominal stress approach, and the structural hot spot stress approach.

Nominal stress is the stress level calculated based on the sectional area under consideration. It accounts for stress-raising effects due to the component's macro-geometric shape near the joint but excludes the
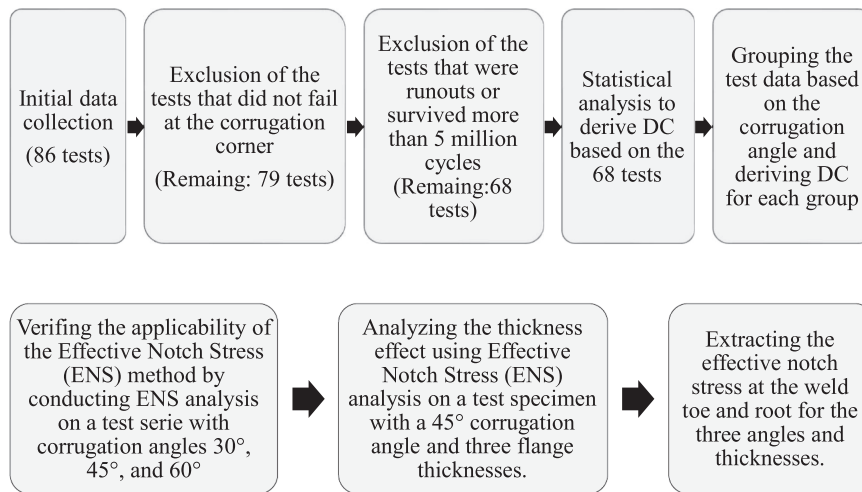
Fig. 2. An overview of the methodology used in this study.

local stress concentration effects from the welded connection [25]. In simple components, nominal stress can be determined using basic structural mechanics theories assuming linear-elastic behaviour. It represents the average stress in the weld throat or plate at the weld toe, as specified in structural detail tables. In more complex cases, Finite Element Method (FEM) modelling may be used [25].

The structural or geometric stress σ_{hs} at the hot spot includes all stress raising effects of a structural detail excluding that due to the local weld profile itself. The non-linear peak stress σ_{nlp} caused by the local notch, i.e. the weld toe, is excluded from the structural stress [25]. The non-linear peak stress is instead avoided by linearizing the stress through the plate thickness or by extrapolating the stress at the surface to the weld toe. This approach is confined to assessing the weld toe as a

location for crack propagation [25].

Effective notch stress is the stress observed at the root of a notch, based on the assumption of linear-elastic material behavior. To accommodate the variations in weld shape and the non-linear behavior of materials at the notch root, the real weld contour is substituted with an effective one. Studies have shown that for structural steels and aluminum alloys, an effective notch root radius of r = 1 mm yields consistent results. In fatigue assessment, the effective notch stress is evaluated against a single fatigue resistance curve, but it is important to verify that this curve does not surpass the fatigue resistance of the parent metal [25]. This method can be used for the assessment of welded joints with respect to potential fatigue failures from the weld toe or weld root [25]. The method is limited to thicknesses t > = 5 mm, since the method

(a) 4-point bending

(b) 3-point bending

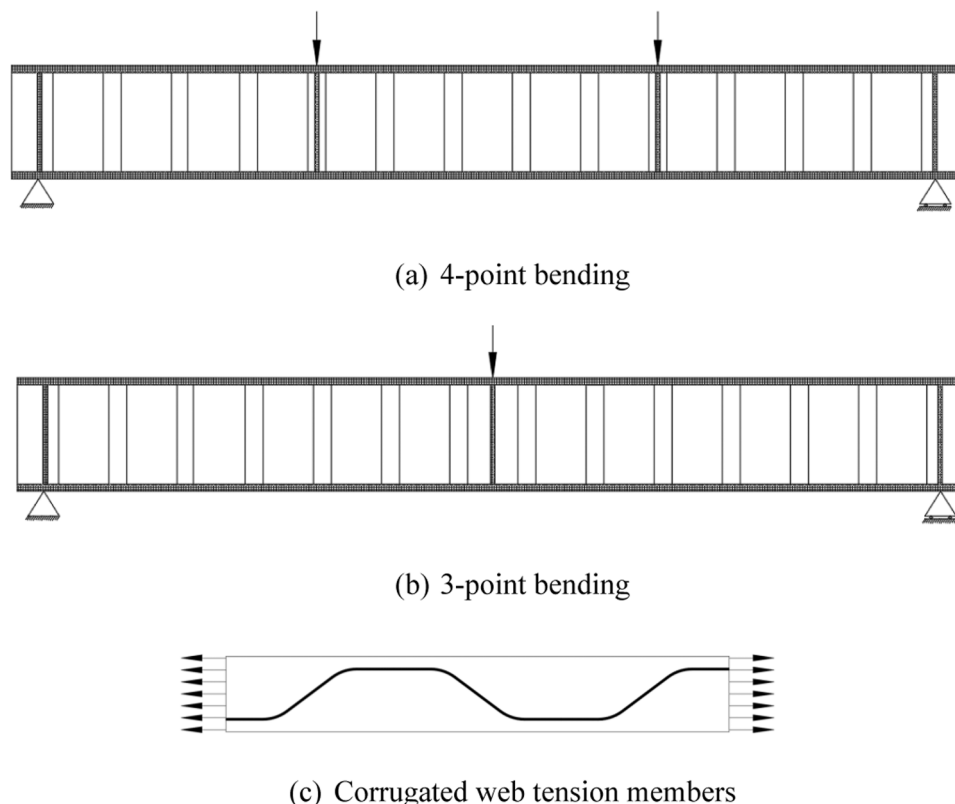(c) Corrugated web tension members

Fig. 3. Overview of the types of test specimens used to evaluate the fatigue performance of the welded connection between flange and corrugated web.

has not yet been verified for smaller wall thicknesses [25]. More details about this method can be found in IIW [25].

3. Overview of previous investigations

3.1. Previous experimental research on the fatigue strength of corrugated web girders

Reported fatigue tests which aim at studying the fatigue performance of the web-to-flange weld in girders with corrugated web can be arranged in three different categories. Beam tests include welded beams tested under 4- and 3-point bending (Figs. 3a and 2b), and test specimens made of T-section members built up of a flange plate and a welded corrugated web and loaded in tension (Fig. 3c). In total, 86 tests were collected, comprising 25 beams and 61 tension members. Of the tension members, 41 were conducted by Wang et al. [16], and 20 by Tong et al. [17]. Among the 25 beam tests, 20 were subjected to four-point bending (6 by Ibrahim et al. [20], 8 by Sauce et al. [21], 2 by Kövesdi and Dunai [15], 1 by Xu et al. [23], 2 by Kotaki et al. [22], and 1 by Tong et al. [17]), while 5 were tested under three-point bending (1 by Wang et al. [24] and 4 by Kövesdi and Dunai [15]). Regarding welding method, most of the reported tests were conducted using semiautomatic gas metal weld welding technique. An overview of the geometrical parameters' ranges in the collected test specimens are summarized in Table 1. The nominal stress with the corresponding number of cycles to failure and crack location from these experimental studies are summarized in Table 6 in Annex A.

3.2. Parameters influencing the fatigue strength of corrugated web girders

In addition to flange thickness, web thickness, and weld throat thickness, which are present in flat web girders, the corrugated web introduces additional parameters that might influence the stress concentration in the flange-to-web connection in beams with corrugated webs, and thus their fatigue strength. These parameters include the corrugation angle (α), the bend radius (R), the corrugation depth (a3), and the lengths of the flat (a1) and inclined folds (a2), see Fig. 4.

The effect of several influential geometrical parameters on stress concentration at the fatigue critical point, such as the corrugation angle and the bend radius has been investigated in previous studies. Xu et al. [23] conducted an effective notch stress analysis on girders with webs having different corrugation angles. Their findings indicated that increasing the angle from 30° to 60° results in approximately a 30 % increase in the stress concentration at fatigue critical point. Wang et al. [16] conducted an experimental program on corrugated web T-section members (CWT), demonstrating that an increase in corrugation angle from 30° to 45° and 60° resulted in a noticeable reduction in fatigue strength.

Anami et al. [26] conducted a parametric finite element method (FEM) analysis, revealing that the corrugation angle and the bend radius at the fold lines of the corrugations significantly influence the stress at the web-flange weld toe. Specifically, increasing the corrugation angle from 25° to 36.7° raised the stress concentration at the S-point from 1.4 to 1.85 (32 %). Altering the radius from 120 mm to 60 mm (halving the radius) increased the stress concentration factor from 1.8 to 1.95 (8 %). The effects of flange thickness and flange width were found to be less

Table 1
Geometrical parameters included in the test database.

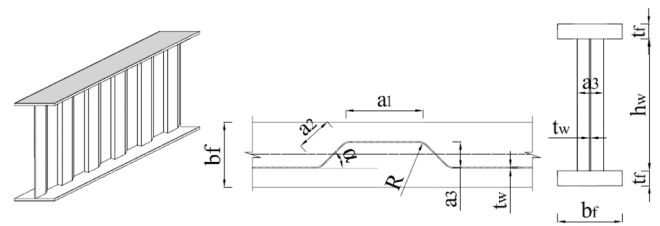| Parameter	Symbol	Range
Corrugation angle	α	30 −60 degrees
Web plate thickness	t_w	3 to 6.4 mm
Flange plate thickness	t_f	6 to 25 mm
Corrugation bend radius	R	27 to 120 mm
Weld throat thickness	a_w	3 to 8 mm

Fig. 4. Geometrical parameter of girders with corrugated webs.

significant than the angle and bend radius effect.

Wang et al. [16] conducted a parametric finite element analysis to examine the impact of geometrical parameters on the stress concentration at the fatigue critical point. The results indicated that the ratio of bend radius to corrugation depth has a more significant effect when the corrugation angle is larger. They also concluded that fatigue strength is more sensitive to the corrugation angle and the ratio of bend radius to corrugation depth than to the length of the longitudinal fold and the width or thickness of the flange.

Regarding weld size, Xu et al. [23] using effective notch stress analysis, showed that the SCF is – in principle – insensitive to weld size. When the latter was changed from 6 to 10 mm the stress concentration increased by only 2.1 % at the failure location.

Sauce et al. [21] conducted an experimental study examining the impact of welding techniques on the fatigue strength of corrugated web girders. Their findings revealed that Robotic Gas Metal Arc Welding (GMAW) improved fatigue life by 42 % compared to semiautomatic GMAW. This enhancement is attributed to the consistent welding toe geometry achieved with the robotic process.

4. Statistical analysis of previous fatigue tests

The nominal stress, number of cycles to failure, and crack location from previous experimental studies are summarized in Annex A. Values were extracted from tables in respective papers, except for Wang et al. [16], where values were obtained from Fig. 8 in [16]. For the girder tests like the ones reported by Ibrahim et al. [20] and Sauce et al. [21], nominal stress was calculated by the authors using simple beam theory ($\sigma = M/W$), providing an average stress in the flange and ignoring the web contribution to the section modulus. Kövesdi and Dunai [15] considered a portion of the web in calculating the beam section modulus (3/20 of the web depth). This consideration was based on stress measurements.

For Tong et al.'s CWT experiment, the authors reported that the nominal stress was obtained from FE analysis where a flat web tension member (FWT) with the same dimensions as the corrugated member was modelled, and nominal stress was read at the top surface of the flange [17]. This stress closely matched the average stress measured at the top surface of the flange, taken from a section in the middle of the flat fold during the experiment (Fig. 12 and 14 in [17]).

4.1. Evaluation of previous experiments with nominal stress method

Out of the 86 test specimens that are collected and stipulated in Annex A, 7 tests were excluded due to failure reported elsewhere than the detail studied here. The remaining 79 tests are plotted in Fig. 5. These include 8 run-outs and two beams that failed at more than 5 million cycles, which all are excluded from the statistical analysis according to [27]. The resulting mean S-N curve from the regression analysis assuming a slope of 3 according to the IIW recommendations [25] is presented in the same figure.

According to Drebenstedt and Euler [27], an outlier is defined as a data point significantly greater or smaller than the rest, lying three or more standard deviations from the sample mean. Thus, the test results were plotted with the mean curve along with ± 3 standard deviations to
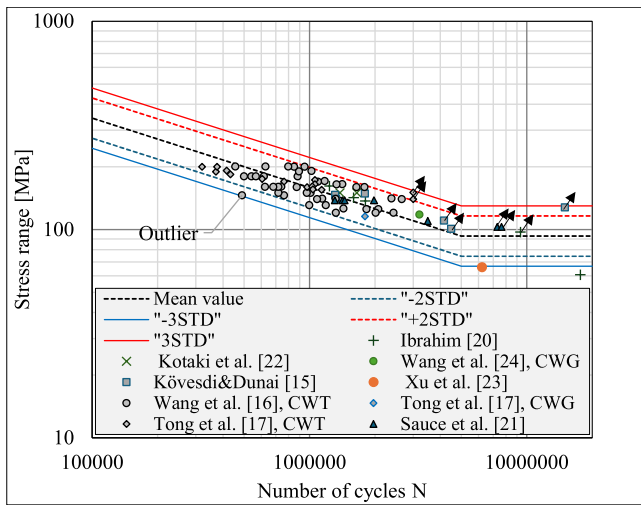
Fig. 5. The collected (79) experimental results including those with reported fatigue cracks at the S-point (68) Runouts and failure above 5 million cycles (10) and 1 outlier.

identify outliers. As shown in Fig. 5, one outlier was observed: a girder tested by Wang et al. [16] which deviated by three standard deviations from the mean curve and was therefore excluded from the following statistical analysis. This outlier corresponds to one of the tension members tested by Wang et al. [16], which was of corrugation angle 60 degrees. The specimen was subjected to a stress range of 145.9 MPa and exhibited a fatigue life of 489 261 cycles.

The remaining tests that are evaluated are plotted in Fig. 6. Using the Eurocode 0 resistance model approach (Section D8.2, Annex D of EN1990:2002), explained further in [27], the detail category for the collected corrugated web girders is estimated to be 100.5 MPa. Consequently, the characteristic detail category can be rounded to 100 MPa in EN1993–1-9.

4.2. Evaluation of the effect of influential corrugation geometric parameters

4.2.1. The effect of corrugation angle

As mentioned in Section ⌐3.2, the corrugation angle is expected to significantly affect the fatigue strength of corrugated web girders. Consequently, the results shown in Fig. 6 are grouped and re-analyzed in
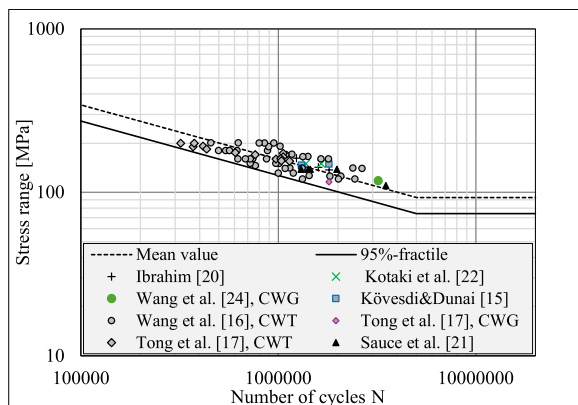
Number of tests: 68
Standard deviation: 0.145
Detail category: 100.5 MPa
Mean S-N curve: LogN =12.605-3.Log S

Fig. 6. S-N relation of test results from literature data.

four groups based on the corrugation angle in the tested specimens. The first group consists of specimens with a corrugation angle of 30°, which includes those tested by Kotaki et al. [22] and Wang et al. [24]. The second group comprises beams with corrugation angles ranging from 37° to 39°, tested by Sauce et al. [21], Kövesdi and Dunai [15], and Ibrahim et al. [20]. The third group includes test specimens with a corrugation angle of 45°, as tested by Wang et al. [16] [24] and Tong et al. [17]. The fourth group includes tests specimens with an angle of 60° tested by Wang et al. [16]. The statistical analysis results for these groups are summarized in Fig. 7.

Comparing Fig. 7 to Fig. 6 reveals that the scatter for the four categories with different corrugation angles is significantly smaller than the scatter when all corrugation angles are considered together. The standard deviation decreased from 0.145 for all girders to 0.055, 0.076, 0.096, and 0.083 for the girders with corrugation angles of 30°, 37–39°, 45°, and 60°, respectively. This indicates that the fatigue strength of corrugated web girders is largely influenced by the corrugation angle, allowing for the assignment of four distinct SN curves for the different angles, as seen in Fig. 8.

The characteristic detail categories derived from statistical analysis and presented in Fig. 7, need to be rounded to the standard detail categories (DC) in EN1993–1-9. Therefore, the recommended detail categories for the use in fatigue design of beams with corrugated webs are presented in Table 2.

4.2.2. The effect of corrugation bend radius

To analyse the effect of bend radius, girders with similar corrugation angles but different radii were grouped and analysed. Specifically, girders tested by Ibrahim et al. [20] and Sauce et al. [21] share a corrugation angle of 36.9° degrees but differ in bending radius (R). Ibrahim's girders have R= 27 mm and Sauce et al.'s girders have R= 120 mm. The results are presented in Fig. 9a. The scatter between the two radii is small, suggesting that a single detail category can be assigned for both radii.

A similar finding was observed when considering the tension specimens tested by Tong et al. [17], which all had a corrugation angle of 45° but varying bending radii (R=30 mm and R=60 mm). These results are presented in Fig. 9b. The small scatter in these tests supports the earlier conclusion from the Ibrahim et al. [20] and Sauce et al. [21] specimens, that a single detail category can accommodate different bending radii. Notably, Tong et al. [17] measured the structural hot spots close to the S-points in specimens with identical corrugation but with different bend radii (30 mm and 60 mm). The results indicated that the stress concentration factor (SCF) for the 30 mm radius, increased by 9 % compared to the case with a bend radius of 60 mm. This difference is not reflected in the test results and has only negligible effect on the regression analysis, as it would result in very close S-N curves.

A similar observation was noted in the numerical study conducted by Anami et al. [26]. Increasing the radius from 60 mm to 180 mm (a factor of three) resulted in a decrease in the stress concentration factor by approximately 8 %. In this study, where the corrugation angle was smaller (37° compared to 45° in Tong's study), the stress concentration sensitivity to the bend radius was less pronounced. This suggests that the impact of the bend radius becomes more significant with larger corrugation angles. However, this requires a more detailed investigation.

5. Investigation of fatigue strength using effective notch stress analysis

By analyzing the experimental data, two key questions arise. The first question is whether a substantial thickness effect exists in the studied welded detail, such that beams with thicker flanges are expected to have lower fatigue strength than beams with identical corrugated webs but with smaller flange thickness. Flange thicknesses included in the test data range from 6 to 25 mm, which is relatively small compared to flange thicknesses typically found in bridge applications. The second
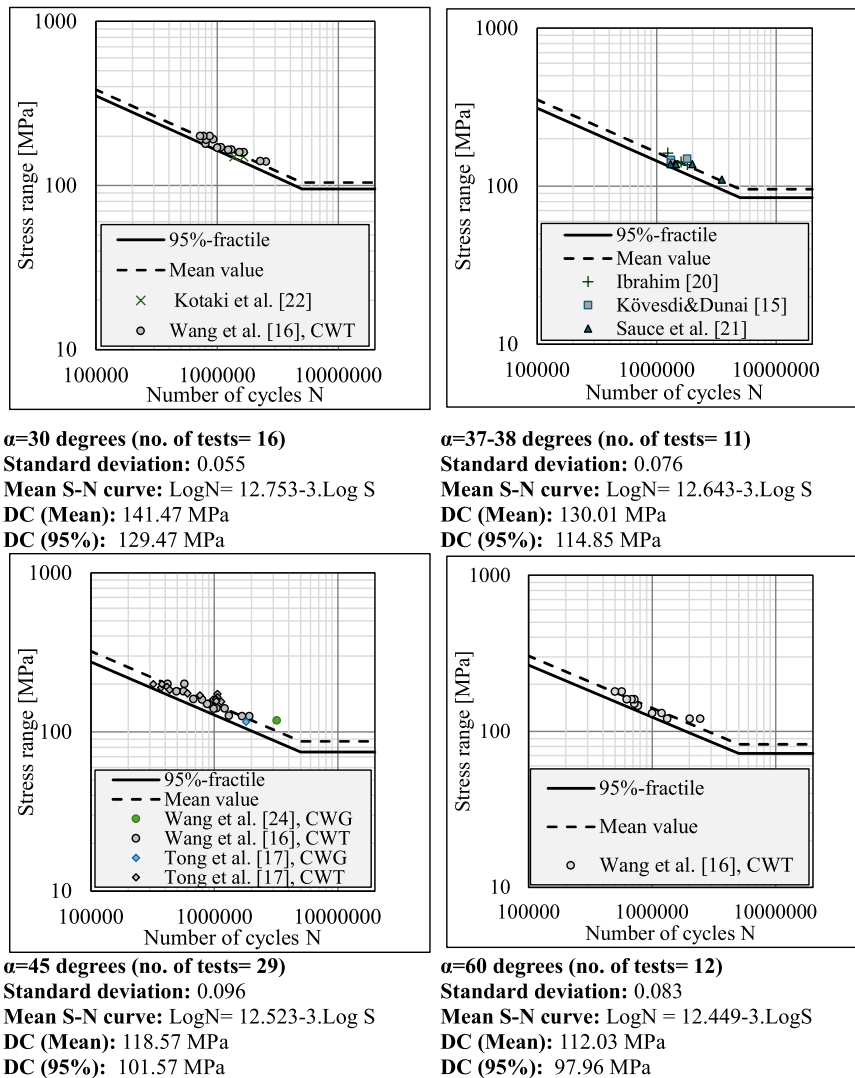
α=30 degrees (no. of tests= 16)
Standard deviation: 0.055
Mean S-N curve: LogN= 12.753-3.Log S
DC (Mean): 141.47 MPa
DC (95%): 129.47 MPa

α=37-38 degrees (no. of tests= 11)
Standard deviation: 0.076
Mean S-N curve: LogN= 12.643-3.Log S
DC (Mean): 130.01 MPa
DC (95%): 114.85 MPa

α=45 degrees (no. of tests= 29)
Standard deviation: 0.096
Mean S-N curve: LogN= 12.523-3.Log S
DC (Mean): 118.57 MPa
DC (95%): 101.57 MPa

α=60 degrees (no. of tests= 12)
Standard deviation: 0.083
Mean S-N curve: LogN = 12.449-3.LogS
DC (Mean): 112.03 MPa
DC (95%): 97.96 MPa

Fig. 7. Evaluation of corrugation angle with nominal stress method.
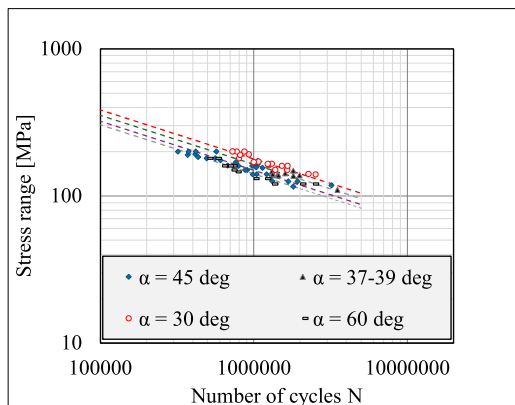
Fig. 8. Mean SN curves for α = 30, 38, 45, and 60 degrees.

Table 2
Proposed detail categories for different corrugation angles.

Corrugation angle	DC
$\alpha \leq 30$	125
$30 < \alpha \leq 40$	112
$40 < \alpha \leq 45$	100
$45 < \alpha \leq 60$	90

a single S-N curve. The ENS is also capable of capturing the thickness effect in welded joints (i.e., stress concentration/gradient). Furthermore, it can be used to assess welded joints for potential fatigue failures originating from the weld toe or weld root [25].

Initially, the tests performed by Wang et al. [16] are used to verify that the ENS method captures the effect of the corrugation angle and confirms the validity of the IIW's proposed detail category (DC225) with the maximum principal stress for ENS analysis of this type of detail. These tests include corrugation geometries with different angles (30°, 45°, 60°). Following this verification, the specimen with angle 45 is then analyzed with larger flange thicknesses to study the effect of flange thickness on the stress concentration factor (SCF). Additionally, the relation between notch stresses at the weld toe and weld root is investigated for the three specimens with different corrugation angles.

question is whether – owing to the complex force transfer in the welded joint between the flange and corrugated web – there is a risk of root cracking in this type of detail.

In order to shed some light on the aforementioned two questions, the effective notch stress (ENS) method is employed. This method is capable of capturing stress concentration effects accurately and relating those to

Standard deviation: 0.069 (no. of tests= 11)
Mean S-N curve: LogN = 12.66-3LogS
DC (Mean): 131.72MPa
DC (95%): 117.54 Mpa
(a)

Standard deviation: 0.1 (no. of tests= 14)
Mean S-N curve: LogN = 12.542-3LogS
DC (Mean): 120.32 Mpa
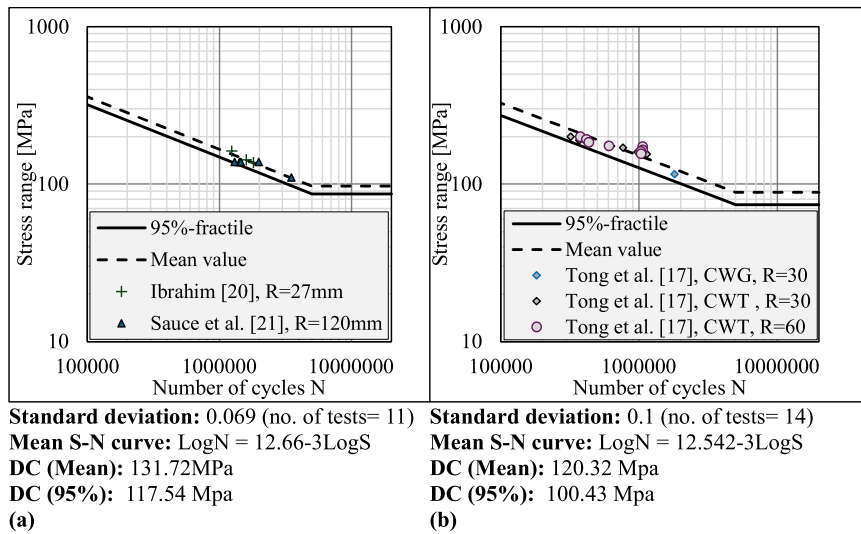**DC (95%):** 100.43 Mpa
(b)

Fig. 9. Evaluation of corrugation bending radius with nominal stress method.

A detailed description of the finite element model and its results is provided in the following sections.

5.1. Finite element model description

The CWT tension members test specimens with angles 30°, 45°, and 60° from Wang et al. [16] were modelled using ABAQUS CAE2023 [28]. A tension force was applied to one of the flange edges. In the original experiments, the specimens were clamped at one end and subjected to axial tension on the other end.

To replicate these conditions in the numerical model, boundary conditions were carefully defined. Fig. 10 shows the applied boundary conditions in the global model. One end of the flange plate is fully constrained, with all movement and rotation restricted, representing a clamped end. The other end is fixed except for movement in the x-direction, allowing the specimen to move only along this axis, matching the experimental setup. To simulate the clamped edge where the load is applied, a reference point at the center of the flange was chosen as the master point, and all surface nodes were linked to it using a multi-point constraint (MPC), as shown in Fig. 10a. This ensured that all points on the loaded edge moved uniformly in the x-direction. The global model uses ten-node quadratic tetrahedral elements (C3D10) to capture the geometry and stress distribution, with a 1.5 mm mesh size, providing four elements through the thickness.

To evaluate the effective notch stress (ENS), a detailed sub-model was created around the S-point (Fig. 10c). This finite element (FE)

sub-model utilized a highly dense mesh in critical areas around the weld toe and root, while a coarser mesh was applied to the rest of the specimen. The modelling of the weld configuration is conducted according to IIW recommendation [25], i.e., the weld toe and root are rounded with radius r = 1 mm. Quadratic tetrahedral solid elements (C3D10) were employed for modelling. These elements simplify the sub-modelling process for the effective notch model. A mesh convergence study showed that the element size 0.25 mm inside the root and toe regions, gradually increasing to 1 mm towards the outer edges captures the effective notch stress with good accuracy. This meshing approach is illustrated in Table 3.

5.2. DC225 with effective notch stress for the three corrugation angles

The effective notch stress results at the weld root and weld toe from the three FE models for the three corrugation angles are presented in Table 4. The nominal stress at the top surface of the flange is defined as the average stress along a path that runs along the flange width at the middle of the flat fold. The obtained nominal stress complies with that calculated by Tong et al. [17]. Moreover, calculating the nominal stress using the formula $\frac{M}{W} + \frac{N}{A}$ where M is the moment caused by the eccentricity resulting from the shift in the neutral axis due to the presence of the web, yields result very close to those obtained in the current approach.

The fatigue life reported by Wang et al. [16] is plotted with reference to the maximum principal effective notch stress obtained from the finite element analysis, which was consistently found in the S-point area in all three models. The results are presented in Fig. 11b. For the sake of comparison, the fatigue life results with reference to the nominal stress component are also plotted in Fig. 11a. As can be observed in Fig. 11, the scatter of the fatigue life decreases significantly when using the effective notch stress method, reducing the standard deviation from 0.17 to 0.09. Additionally, all results lie above DC 225, indicating that DC 225 suggested by IIW [25] with the maximum principal effective notch stress provides a good representation of the fatigue strength for this type of detail.

5.3. Effect of flange plate thickness

According to Pedersen [29] the thickness effect is considered to be a compound effect caused by: the geometric size effect, statistical size effect, and technological size effect. The geometric size effect encompasses two issues that lead to poorer conditions for thicker joints: the stress gradient effect and the effect of incomplete scaling. The stress
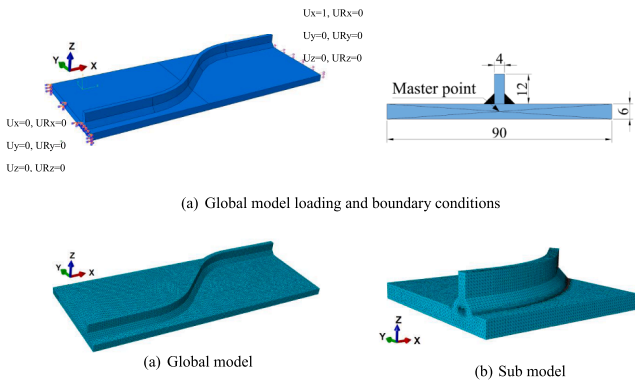

(a) Global model loading and boundary conditions

(a) Global model

(b) Sub model

Fig. 10. FE model and boundary conditions of the considered CWT test specimen.

Table 3

Mesh sensitivity on ENS.
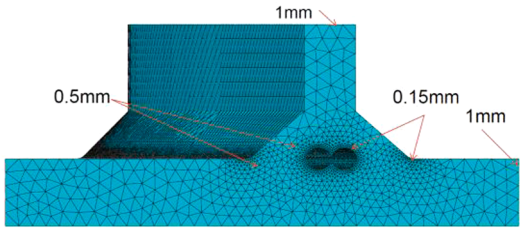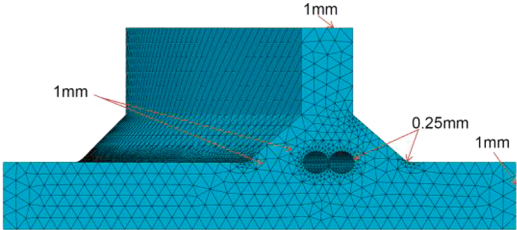
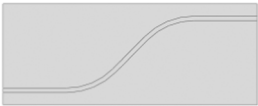| Mesh size		

ENS_{Toe}	266.1 Mpa	264.9 Mpa
ENS_{Root}	210.7 Mpa	208.4 Mpa

Table 4

Effective notch stress at weld toe and root in the S-point area for angles α = 30°, 45°, 60° obtained from FE analysis.

		Nominal stress [MPa]	ENS_{Toe} [MPa]	ENS_{Root} [MPa]	SCF_{Toe}	ENS_{Toe}/ ENS_{Root}
α = 30°		161.50	264.9	208.4	1.64	1.27
α = 45°		158.14	328.72	250.5	2.08	1.31
α = 60°		158.93	395.94	307.88	2.49	1.29

(a) Nominal stress
Standard deviation: 0.17
No. of tests= 40

(b) Effective notch stress
Standard deviation: 0.09
No. of tests= 40
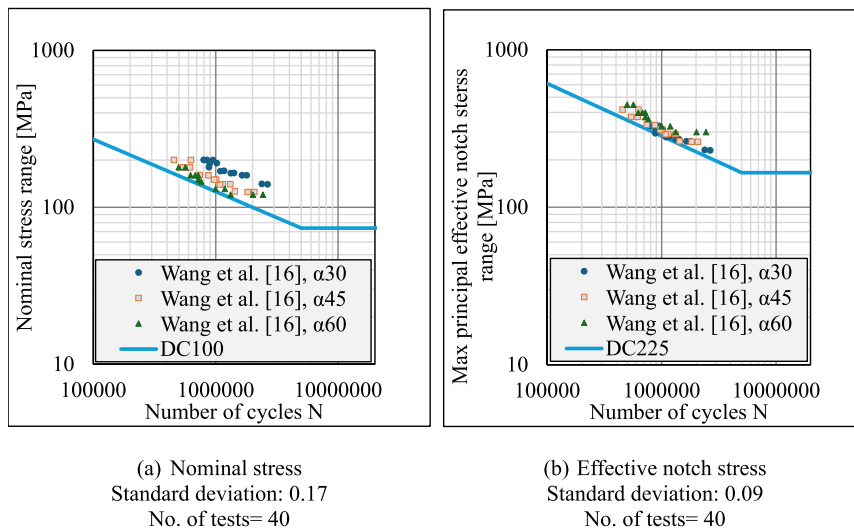
Fig. 11. Fatigue life as a function of normal stress and effective notch stress.

gradient is steeper in thinner joints, reducing the intensity of the combined stress field at the crack tip for a given crack size. In terms of incomplete scaling, fatigue is considered the weakest link process, where cracks initiate and grow in areas with the worst combination of detrimental effects, such as stress concentration, weld defects, residual stresses, and material properties. The weld toe's radius remains constant regardless of plate thickness, causing the ratio between the toe radius and plate thickness to decrease, which increases stress concentration [29].

The statistical size effect indicates that the probability of severe

defects is higher in larger volumes (thick joints) than in smaller volumes (thin joints). The technological size effect suggests that larger/thicker structures provide greater constraints against the thermal contraction of weld material compared to smaller/thinner structures, leading to higher residual stress levels [29].

To investigate the technological and statistical effects, fatigue testing is required. This section, however, focuses solely on the geometric effect.

The specimen with a corrugation angle of 45° from Wang et al. [16] is modelled with increasing flange thicknesses from 6 mm to 24 mm, and up to 48 mm (approximating real bridge girder applications). The

effective notch stress at the root and the toe were extracted and presented in Table 5. By comparing the stress concentration factor at the weld toe, it can be observed that the stress concentration factor remains around 2 for all three thicknesses. This indicates that the stress concentration for the studied detail is not sensitive to flange thickness. However, further studies are needed to confirm this observation.

5.4. Root vs toe cracking

None of the experimental fatigue investigations included in the current study reported root cracking. Nevertheless, to assess the risk of root cracking, the root effective notch stress (ENS_{Root}) was extracted from finite element analysis and presented for the three corrugation angles in Table 4 and the three thicknesses in Table 5. The modelled specimens have a weld throat thickness of $a_w = 3$ mm and a web plate thickness of $t_w = 4mm$ mm, resulting in a ratio of $2a_w/t_w = 1.5$.

As shown in Table 4 and Table 5, the ratios between the effective notch stress at the weld toe (ENS_{Toe}) and the effective notch stress at the weld root (ENS_{Root}) for the three corrugation angles and the three different thicknesses are approximately 1.3 (not affected by the corrugation angle and flange thickness). This indicates that, in order to avoid root cracking, the ratio $\frac{2a_w}{t_w}$ needs to be at least 1.15. Further analysis is however needed to confirm and generalize this conclusion.

It is worth mentioning here that in the collected studies where the weld throat thickness of the tested specimens was reported, none had a ratio less than 1.15, except for the two specimens tested by Kövesdi et al. [15], which had a smaller weld size of 3 mm. None of these tests were reported to have fatigue cracks initiating from the weld root.

6. Discussion

6.1. Load effects in beams with corrugated webs

The term "nominal stress" used in this paper refers to the primary bending stress in beams or the axial stress in tension specimens. In real bridges with corrugated webs, a transverse bending component, shown in Fig. 12, might be present due to shear flow in the web [12,14,30]. This component is not present in the fatigue tests included in the statistical analysis, except for three beams from Kövesdi and Dunai [15] and one beam from Wang et al.[24]. Therefore, in the fatigue design of real bridge girders, the nominal stress used in fatigue design should include not only the primary bending stresses but also possible transverse bending stress in the flange at the presumed crack initiation point (the S-point).

6.2. The limitation of corrugation parameters

Both statistical analysis of test data and previous analytical work indicate that the corrugation angle is the most influential parameter affecting stress concentration at the S-point. The fatigue test data

included in this paper covers corrugation angles ranging from 30° to 60°. Data for larger corrugation angles is not available, but it is expected that these angles would result in lower fatigue strength. To mitigate this, increasing the radius—which has been shown to be more effective for larger corrugation angles—could enhance fatigue strength. Nonetheless, a comprehensive parametric study is necessary to establish a clear relationship between the stress concentration factor (SCF) at the S-point and the various geometric parameters presented in Fig. 4 before a more detailed assessment of the influence of these corrugation parameters on fatigue strength can be made.

The web thickness in the collected database ranges from 3 to 6 mm. However, in bridge application, larger web thicknesses might be needed. Therefore, the influence of the web thickness on the fatigue strength needs to be investigated in a more detailed study and verified by testing.

7. Summary and conclusions

This paper aims at deriving detail categories for the flange-to-web weld detail in corrugated web beams. Test data from previous studies are collected and analyzed. A statistical analysis is conducted to establish 4 detail categories that can be used in the fatigue design of these elements.

Moreover, effective notch stress (ENS) analysis is conducted on tension test specimens having webs with different corrugation angles to verify the applicability of the detail category proposed in the IIW recommendations for fatigue analysis with this method (i.e. DC225 using the principal stress). Additionally, the possible thickness effect is examined using the ENS method, and the same FE models are used to evaluate the risks of root cracking in the studied detail. The following conclusion can be drawn:

- Analysis of the experimental data and previous analytical studies indicates that the corrugation angle is the most influential geometrical parameter. It also suggests that the fatigue strength might also be affected by the bend radius, especially for larger corrugation angles. Further analysis is required to quantify this effect.
- The statistical analysis of the collected test data, comprising 68 tests, indicates that a detail category of 100 MPa can be used if all test data are included in the analysis irrespective of the corrugation geometrical parameters.
- The fatigue life of corrugated web girders is found to be significantly influenced by the corrugation angle, allowing for different detail categories to be assigned to weld details with different corrugation angles. This study proposes DC125 for angles smaller than 30°, DC112 for angles between 30° and 40°, DC100 for angles between 40° and 45°, and DC90 for angles between 45° and 60°, which are summarized in Table 2.
- DC225, using maximum principal effective notch stress at the weld toe, accurately represents the fatigue life of the flange-to-web detail in corrugated web girders. Evaluation of fatigue tests with test

Table 5

Effective notch stress at weld toe and root in the S-point area for angle α = 45° and flange thickness $t_f = 6mm$, $24mm$, $48mm$ obtained from FE analysis.

		Nominal stress [Mpa]	ENS_{Toe} [Mpa]	ENS_{Root} [Mpa]	SCF_{Toe}	ENS_{Toe}/ ENS_{Root}
α = 45°, $t_f = 6mm$		158.14	328.72	250.5	2.08	1.31
α = 45°, $t_f = 24mm$		175.76	348.88	259	1.98	1.35
α = 45°, $t_f = 48mm$		176.80	349.97	265.12	1.98	1.32

$$(a) \quad M_{\max} = \frac{V \cdot a_3}{4 \cdot h_w} \cdot (2 \cdot a_1 + a_4)$$

$$(b) \quad M_{\max} = \frac{V \cdot a_3}{2 \cdot h_w} \cdot (2 \cdot a_1 + a_4)$$
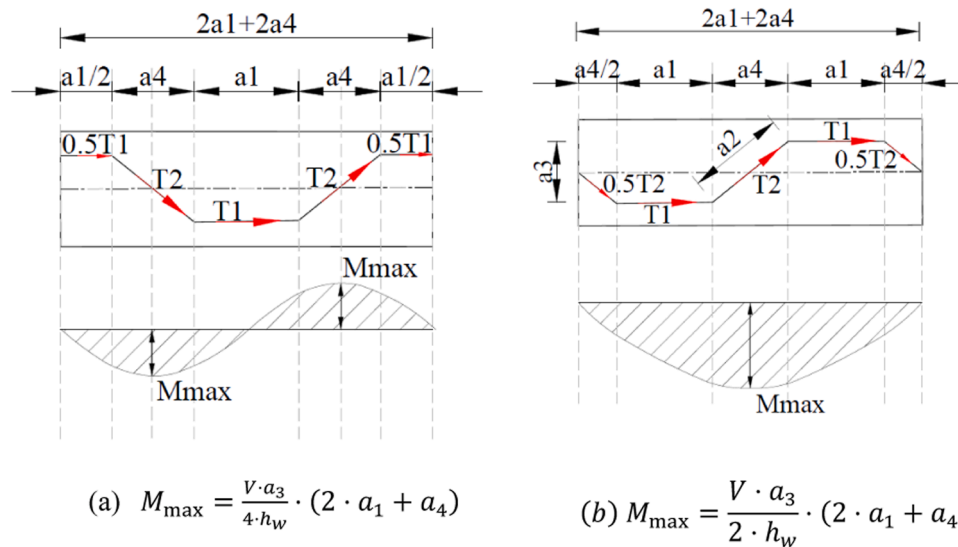
Fig. 12. Transverse bending from shear flow according to Kövesdi et al. [14]: (a) when the load and supports are located on the flat fold, (b) when the load and supports are located on the inclined fold.

specimens having different corrugation geometries showed a substantial reduction in scatter compared to that obtained from the nominal stress method.

- The test data is limited in the range of flange thickness, and no obvious thickness effect could be recognized from analysing the tests. Furthermore, ENS analysis of corrugations with various angles shows that the stress concentration factors are not influenced by flange thickness, and as such no thickness correction is required.
- ENS analysis of weld details in corrugated webs having different corrugation angles shows that root cracking can be avoided if the ratio between weld throat thickness and web thickness ($\frac{2a_w}{t_w}$) is larger than 1.15. Examination of the fatigue test data shows that out of the 86 tests, only 2 specimens did not fulfil this requirement. No root cracking was reported for any of the tests.

Furthermore, the following points are recommended for further research:

- Tests with angles larger than 60 degrees, flanges over 20 mm, and web thicknesses greater than 6 mm are needed to extend the applicability of the proposed detail categories.
- Additional fatigue testing, including transverse bending, is necessary to evaluate its impact on fatigue life and determine the stress concentration caused by transverse bending.
- A more detailed analysis to study the influence of various geometric parameters on the stress concentration in beams with corrugated webs would also be beneficial to support and validate an extension of

the proposed detail categories to girders with other geometric parameters than those included in the collected tests.

CRediT authorship contribution statement

Mohammad Al-Emrani: Writing – review & editing, Visualization, Supervision, Methodology, Funding acquisition. **Fatima Hlal:** Writing – review & editing, Writing – original draft, Visualization, Software, Methodology, Formal analysis, Data curation.

Declaration of Competing Interest

The authors declare that they have no known competing financial interests or personal relationships that could have appeared to influence the work reported in this paper.

Annex A

Table 6
The collected experimental database.

Ref.	Specimen	Loading type	L [mm]	b_f [mm]	t_f [mm]	h_w [mm]	t_w [mm]	a_3 [mm]	a_1 [mm]	α [deg]	R [mm]	a_w [mm]	$\Delta\sigma_{nom}$ [MPa]	N	Comment
[20]	CWG2 −1	4-point	6076	150	12.7	500	3	75	117	36.87	27	5	97	2160000	Crack at stop/start point
[20]	CWG2 −2	4-point	6076	150	12.7	500	3	75	117	36.87	27	5	65	17613800	Fatigue crack at S-point

Table 6 (*continued*)

Ref.	Specimen	Loading type	L [mm]	b_f [mm]	t_f [mm]	h_w [mm]	t_w [mm]	a_3 [mm]	a_1 [mm]	α [deg]	R [mm]	a_w [mm]	$\Delta\sigma_{nom}$ [MPa]	N	Comment
															(above 5 million cycles)
[20]	CWG2 −3	4-point	6076	150	12.7	500	3	75	117	36.87	27	5	142	1595000	Fatigue crack at S-point
[20]	CWG2 −4	4-point	6076	150	12.7	500	3	75	117	36.87	27	5	137	1806100	Fatigue crack at S-point
[20]	CWG2 −5	4-point	6076	150	12.7	500	3	75	117	36.87	27	5	162	1235100	Fatigue crack at S-point
[20]	CWG2 −6	4-point	6076	150	12.7	500	3	75	117	36.87	27	5	97	9339000	Run-out
[21]	G2A	4-point	7400	227	20	1200	6	150	300	36.9	120	8	138	1418000	Fatigue crack at S-point
[21]	G1A	4-point	7400	227	20	1200	6	150	300	36.9	120	8	138	1448000	Fatigue crack at S-point
[21]	G4A	4-point	7400	227	20	1200	6	150	300	36.9	120	8	138	1304000	Fatigue crack at S-point
[21]	G6A	4-point	7400	227	20	1200	6	150	300	36.9	120	8	103	2563000	Different weld on different sides
[21]	G4B	4-point	7400	227	20	1200	6	150	300	36.9	120	8	138	1980000	Robotic welding
[21]	G1B	4-point	7400	227	20	1200	6	150	300	36.9	120	8	110	3500000	Robotic welding
[21]	G5A	4-point	7400	227	20	1200	6	150	300	36.9	120	8	103	7317000	Run-out
[21]	G3A	4-point	7400	227	20	1200	6	150	300	36.9	120	8	103	7645000	Run-out
[22]	1	4-point	6500	300	0	600	4.5	75	120	30	75	3	150	1380000	Fatigue crack at S-point
[22]	2	4-point	6500	300	0	600	4.5	75	120	30	75	3	150	1650000	Fatigue crack at S-point
[24]	B4 −45o-n	3-point	1760	88	6	248	4	64	82	45	-	3	160	3200000	Fatigue crack at S-point
[15]	3	3-point	7150	225	20	500	6	133	210	39	60	6	147	1310000	Fatigue crack at S-point
[15]	4	3-point	7150	225	20	500	6	133	210	39	60	6	140	1326000	Fatigue crack at S-point
[15]	5	3-point	7150	225	20	500	6	133	210	39	60	3	149	1800000	Fatigue crack at S-point
[15]	6	3-point	7150	225	20	500	6	133	210	39	60	3	128	15000000	Run-out
[15]	1	4-point	7150	225	20	500	6	133	210	39	60	6	101	4486000	Run-out
[15]	2	4-point	7150	225	20	500	6	133	210	39	60	6	111	4162000	Run-out
[23]	1	4-point	12000	424/ 297	25	1650	6.4	160	340	45	100	7	66	6208700	Fatigue crack at S-point (above 5 million cycles)
[17]	CWG-R30	4-point	3670	150	16	500	5	60	120	45	30	5	116	1800000	Fatigue crack at S-point
[17]	R30 −1	Uniaxial	700	90	8	40	5	60	120	45	30	5	200	320000	Fatigue crack at S-point
[17]	R30 −2	Uniaxial	700	90	8	40	5	60	120	45	30	5	190	370000	Fatigue crack at S-point
[17]	R30 −3	Uniaxial	700	90	8	40	5	60	120	45	30	5	180	789000	Crack in inclined fold
[17]	R30 −4	Uniaxial	700	90	8	40	5	60	120	45	30	5	170	763000	Fatigue crack at S-point
[17]	R30 −5	Uniaxial	700	90	8	40	5	60	120	45	30	5	160	972000	Fatigue crack at S-point
[17]	R30 −6	Uniaxial	700	90	8	40	5	60	120	45	30	5	155	1138000	Fatigue crack at S-point
[17]	R30 −7	Uniaxial	700	90	8	40	5	60	120	45	30	5	153	1140000	Crack in inclined fold
[17]	R30 −9	Uniaxial	700	90	8	40	5	60	120	45	30	5	150	2280000	Run-out (Terminated)
[17]	R30 −8	Uniaxial	700	90	8	40	5	60	120	45	30	5	151	3000000	Crack in inclined fold
[17]	R30 −10	Uniaxial	700	90	8	40	5	60	120	45	30	5	140	3000000	Run-out (Terminated)
[17]	R60 −1	Uniaxial	700	90	8	40	5	60	120	45	60	5	200	375000	Fatigue crack at S-point
[17]	R60 −2	Uniaxial	700	90	8	40	5	60	120	45	60	5	192	415000	Fatigue crack at S-point
[17]	R60 −3	Uniaxial	700	90	8	40	5	60	120	45	60	5	185	672000	Crack at end of parallel fold
[17]	R60 −4	Uniaxial	700	90	8	40	5	60	120	45	60	5	184	433000	Fatigue crack at S-point
[17]	R60 −5	Uniaxial	700	90	8	40	5	60	120	45	60	5	175	605000	Fatigue crack at S-point

Table 6 (*continued*)

Ref.	Specimen	Loading type	L [mm]	b_f [mm]	t_f [mm]	h_w [mm]	t_w [mm]	a_3 [mm]	a_1 [mm]	α [deg]	R [mm]	a_w [mm]	$\Delta\sigma_{nom}$ [MPa]	N	Comment
[17]	R60 −6	Uniaxial	700	90	8	40	5	60	120	45	60	5	173	1059000	Fatigue crack at S-point
[17]	R60 −7	Uniaxial	700	90	8	40	5	60	120	45	60	5	165	1059000	Fatigue crack at S-point
[17]	R60 −8	Uniaxial	700	90	8	40	5	60	120	45	60	5	162	419000	Crack at flange edge
[17]	R60 −9	Uniaxial	700	90	8	40	5	60	120	45	60	5	161	1028000	Fatigue crack at S-point
[17]	R60 −10	Uniaxial	700	90	8	40	5	60	120	45	60	5	156	1035000	Fatigue crack at S-point
[16]	α30 − 1	Uniaxial	160	90	6	12	4	64	82	30	60	3	140	2655763	Most failed at S-point except one from an original notch in the plate edge
[16]	α30 − 2	Uniaxial	160	90	6	12	4	64	82	30	60	3	141	2383358	
[16]	α30 − 3	Uniaxial	160	90	6	12	4	64	82	30	60	3	160	1792354	
[16]	α3 − 4	Uniaxial	160	90	6	12	4	64	82	30	60	3	160	1645977	
[16]	α30 − 5	Uniaxial	160	90	6	12	4	64	82	30	60	3	165	1413916	
[16]	α30 − 6	Uniaxial	160	90	6	12	4	64	82	30	60	3	165	1331753	
[16]	α30 − 7	Uniaxial	160	90	6	12	4	64	82	30	60	3	171	1173314	
[16]	α30 − 8	Uniaxial	160	90	6	12	4	64	82	30	60	3	170	1092482	
[16]	α30 − 9	Uniaxial	160	90	6	12	4	64	82	30	60	3	180	881846	
[16]	α30 − 10	Uniaxial	160	90	6	12	4	64	82	30	60	3	191	1021863	
[16]	α30 − 11	Uniaxial	160	90	6	12	4	64	82	30	60	3	190	894114	
[16]	α30 − 12	Uniaxial	160	90	6	12	4	64	82	30	60	3	200	949323	
[16]	α30 − 13	Uniaxial	160	90	6	12	4	64	82	30	60	3	200	849949	
[16]	α30 − 14	Uniaxial	160	90	6	12	4	64	82	30	60	3	201	798717	
[16]	α45 − 1	Uniaxial	160	90	6	12	4	64	82	45	60	3	125	2072162	
[16]	α45 − 2	Uniaxial	160	90	6	12	4	64	82	45	60	3	125	1825688	
[16]	α45 − 3	Uniaxial	160	90	6	12	4	64	82	45	60	3	126	1433595	
[16]	α45 − 4	Uniaxial	160	90	6	12	4	64	82	45	60	3	140	1319552	
[16]	α45 − 5	Uniaxial	160	90	6	12	4	64	82	45	60	3	141	1143912	
[16]	α45 − 6	Uniaxial	160	90	6	12	4	64	82	45	60	3	140	1082412	
[16]	α45 − 7	Uniaxial	160	90	6	12	4	64	82	45	60	3	150	1009760	
[16]	α45 − 8	Uniaxial	160	90	6	12	4	64	82	45	60	3	150	971232	
[16]	α45 − 9	Uniaxial	160	90	6	12	4	64	82	45	60	3	160	871751	
[16]	α45 − 10	Uniaxial	160	90	6	12	4	64	82	45	60	3	161	741981	
[16]	α45 − 11	Uniaxial	160	90	6	12	4	64	82	45	60	3	180	617153	
[16]	α45 − 12	Uniaxial	160	90	6	12	4	64	82	45	60	3	180	541243	
[16]	α45 − 13	Uniaxial	160	90	6	12	4	64	82	45	60	3	201	455435	
[16]	α45 − 14	Uniaxial	160	90	6	12	4	64	82	45	60	3	201	627181	
[16]	α60 − 1	Uniaxial	160	90	6	12	4	64	82	60	60	3	120	2436709	
[16]	α60 − 2	Uniaxial	160	90	6	12	4	64	82	60	60	3	120	2014602	
[16]	α60 − 3	Uniaxial	160	90	6	12	4	64	82	60	60	3	120	1323881	
[16]	α60 − 4	Uniaxial	160	90	6	12	4	64	82	60	60	3	131	1189575	
[16]	α60 − 5	Uniaxial	160	90	6	12	4	64	82	60	60	3	131	997708	
[16]	α60 − 6	Uniaxial	160	90	6	12	4	64	82	60	60	3	146	763630	
[16]	α60 − 7	Uniaxial	160	90	6	12	4	64	82	60	60	3	146	489261	
[16]	α60 − 8	Uniaxial	160	90	6	12	4	64	82	60	60	3	150	719501	
[16]	α60 − 9	Uniaxial	160	90	6	12	4	64	82	60	60	3	160	719501	
[16]	α60 − 10	Uniaxial	160	90	6	12	4	64	82	60	60	3	160	681127	
[16]	α60 − 11	Uniaxial	160	90	6	12	4	64	82	60	60	3	160	623567	
[16]	α60 − 12	Uniaxial	160	90	6	12	4	64	82	60	60	3	180	566007	
[16]	α60 − 13	Uniaxial	160	90	6	12	4	64	82	60	60	3	180	498854	

Data availability

Data will be made available on request.

References

[1] Wilson, A. (2005) Advances in High Performance Steels for Highway Bridges; National Steel Bridge Alliance (NSBA) White Paper; ⟨https://www.aisc.org/globalassets/nsba/technical-documents/advances-in-high-performance-steels-for-highway-bridges.pdf⟩.

[2] Elgaaly M. Bending strength of steel beams with corrugated webs. J Struct Eng 1997. https://doi.org/10.1061/(ASCE)0733-9445(1997)123:6(772).

[3] Elamary AS, Alharthi Y, Sharaky IA. Behavior of steel beams with different web profiles along the beam length. J Constr Steel Res 2021. https://doi.org/10.1016/j.jcsr.2021.106875.

[4] Abbas HH, Sause R, Driver RG. Behavior of corrugated web I-girders under in-plane loads. J Eng Mech 2006:806–14. https://doi.org/10.1061/(ASCE)0733-9399(2006)132:8(806)#.

[5] Karabulut B, Ferraz G, Rossi B. Lifecycle cost assessment of high strength carbon and stainless steel girder bridges. J Environ Manag 2021. https://doi.org/10.1016/j.jenvman.2020.111460.

[6] Wahlsten, J., Heshmati, M., Al-Emrani, M. (2018) Sustainable Infrastructure through increased use of Stainless Steel; White Paper by Outokumpu;

[7] Zilli, G., Fattorini, F., Maiorana, E. (2008) Application of duplex stainless steel for welded bridge construction in aggressive environment; ⟨https://www.researchgate.net/publication/265668326⟩.

[8] Hechler, O., Collin, P. (2008) On the use of duplex stainless steels in bridge construction; https://api.semanticscholar.org/CorpusID:53077077,

[9] Säll, J., Tiderman, A. (2013) Maintenance-free material in bridge superstructures: Benefits in a cost- and environment prospective in use of stainless steel and directly molded durable concrete; KTH Royal Institute of Technology; ⟨https://kth.diva-portal.org/smash/get/diva2:640396/FULLTEXT01.pdf⟩,

[10] Hlal F, Amani M, Al-Emrani M. Stainless steel corrugated web girders for composite road bridges: optimization and parametric studies. Eng Struct 2023. https://doi.org/10.1016/j.engstruct.2023.117366.

[11] Hlal, F. (2023) Stainless Steel Corrugated Web Girders for Composite Road Bridges: Concept Evaluation and Flange Buckling Resistance; Chalmers University of Technology. Technical Report No ACE 2023:9; ⟨https://research.chalmers.se/publication/536891⟩,

[12] Hlal F., Al-Emrani M. Load effects in beams with corrugated webs: Numerical study; Nordic Steel Construction Conference 2024 (NSCC 2024). The Swedish Institute of Steel Construction; 2024. https://doi.org/10.5281/zenodo.12210008#.

[13] Abbas HH, Sause R, Driver RG. Analysis of flange transverse bending of corrugated web I-girders under in-plane loads. J Struct Eng 2007:347–55. https://doi.org/10.1061/(ASCE)0733-9445(2007)133:3(347)#.

[14] Kövesdi B, Jáger B, Dunai L. Stress distribution in the flanges of girders with corrugated webs. J Constr Steel Res 2012:204–15. https://doi.org/10.1016/j.jcsr.2012.07.023.

[15] Kövesdi B, Dunai L. Fatigue life of girders with trapezoidally corrugated webs: An experimental study. Int J Fatigue 2014:22–32. https://doi.org/10.1016/j.ijfatigue.2014.02.017#.

[16] Wang Z, Wang Q. Fatigue assessment of welds joining corrugated steel webs to flange plates. Eng Struct 2014. https://doi.org/10.1016/j.engstruct.2014.04.041.

[17] Tong L, Zhao Z, Zuo G, Wang H, Pan C. Experimental study on fatigue behavior of trapezoidal corrugated-web girders based on T-section members. Eng Struct 2024. https://doi.org/10.1016/j.engstruct.2023.117078.

[18] Ibrahim SA, El-Dakhakhni WW, Elgaaly M. Fatigue of corrugated-web plate girders: experimental study. J Struct Eng 2006:1371–80. https://doi.org/10.1061/(asce)0733-9445(2006)132:9(1371)#.

[19] Sause R, Abbas HH, Driver RG, Anami K, Fisher JW. Fatigue life of girders with trapezoidal corrugated webs. J Struct Eng 2006. https://doi.org/10.1061/(ASCE)0733-9445(2006)132:7(1070)#.

[20] Ibrahim, S.A.-B. (2001) Fatigue analysis and instability problems of plate girders with corrugated webs; Drexel University; https://doi.org/10.17918/00001482,

[21] Sause, R., Abbas, H.H., Driver, G.R., Anami, K., Fisher, J.W. (2003) Fatigue Resistance of Corrugated Web Girders; ATLSS Reports. Paper 246; ⟨http://preserve.lehigh.edu/engr-civil-environmental-atlss-reports/246⟩,

[22] Kotaki N, Ichikawa A, Sasaki E, Miki C, Hosaka T. Proposal of ripple web bridge and its fatigue strength. J Jpn Soc Civ Eng 2003. https://doi.org/10.2208/jscej.2004.766_233.

[23] Xu J, Sun H, Cai S, Sun W, Zhang B. Fatigue testing and analysis of I-girders with trapezoidal corrugated webs. Eng Struct 2019. https://doi.org/10.1016/j.engstruct.2019.109344.

[24] Wang Z, Tan L, Wang Q. Fatigue strength evaluation of welded structural details in corrugated steel web girders. Int J Steel Struct 2013:707–21. https://doi.org/10.1007/s13296-013-4012-z.

[25] Hobbacher, A.F. (2008) Recommendations for Fatigue Design of Welded Joints and Components; International Institute of Welding; ⟨https://link.springer.com/book/10.1007/978-3-319-23757-2⟩,

[26] Anami K, Sause R, Abbas H. Fatigue of web-flange weld of corrugated web girders: 1. Influence of web corrugation geometry and flange geometry on web-flange weld toe stresses. Int J Fatigue 2005:373–81. https://doi.org/10.1016/j.ijfatigue.2004.08.006.

[27] Drebenstedt K, Euler M. Statistical analysis of fatigue test data according to eurocode 3; Maintenance, Safety. Risk, Management and Life-Cycle Performance of Bridges. Melbourne. Leiden: CRC Press,; 2018. p. 2244–51.

[28] SIMULIA. ABAQUS User's Manual; ⟨http://abaqusdocs.eait.uq.edu.au/v6.11/index.html⟩,

[29] Pedersen MM. Thickness effect in fatigue of welded butt joints. Int J Steel Struct 2019. https://doi.org/10.1007/s13296-019-00254-y.

[30] Abbas HH, Sause R, Driver RG. Simplified analysis of flange transverse bending of corrugated web I-girders under in-plane moment and shear. Eng Struct 2007. https://doi.org/10.1016/j.engstruct.2007.01.006.